Available online at www.sciencedirect.com
ScienceDirect
International Journal of Heat and Mass Transfer 50 (2007) 616–624
International Journal of HEAT and MASS TRANSFER
www.elsevier.com/locate/ijhmt

A mathematical simulation of high temperature induction heating of electroconductive solids

B. Drobenko [a,*], O. Hachkevych [a,b], T. Kournyts'kyi [a]

[a] Institute for Applied Problems of Mechanics and Mathematics, Ukrainian National Academy of Sciences, Naukova Str. 3b, Lviv 79060, Ukraine
[b] Technical University of Opole, Luboszycka Str. 5, Opole 45036, Poland

Received 28 July 2005; received in revised form 11 July 2006
Available online 28 September 2006

Abstract

The mathematical model of non-stationary coupled electromagnetic and thermal processes in polarizable and magnetizable axisymmetric electroconductive solids subjected to electromagnetic field generated by external currents is proposed. The processes parameters are connected through heat sources and temperature dependence of material characteristics. The problem is solved by finite element method. The process of induction heating of a finite steel cylinder is considered.

Keywords: High temperature induction heating; Coupled fields; Finite element method

1. Introduction

Electromagnetic fields are widely used in modern technologies of high temperature heat treatments of solids. In particular, induction heating is frequently applied for hardening, quenching, tempering, melting, brazing and other heat treatments of steels and demands very accurate control of heated depth and surface areas. However, behavior of most steels during the heat treatment is non-linear and very complex. In general, the electromagnetic field distribution in solid depends implicitly on the all past thermal history. Electro-conductive materials can be magnetized or polarized during the process of heat treatment. The magnetic permeability of ferromagnetic materials depends on the magnetic field intensity. Therefore, a practical need arises in development of adequate mathematical models of physical phenomena, which occur during a process of induction heating of solids.

Consideration of above mentioned phenomena that influence time dependent temperature distribution in a solid necessitates development of the complex mathematical models, which are not easy to be analyzed analytically. Because of the temperature-dependence and non-linear properties of most materials during induction heating, analytical solutions of the electromagnetic and temperature distributions are very difficult to obtain. When solids with complex geometrical shapes are considered, the problems become more cumbersome. That caused intensive application of numerical methods, the finite elements method being the most widely used [1–7].

Because in the finite element method the external medium domain is also meshed and the electromagnetic equation is solved on the global domain made out of the external medium, the inductor and the solid, some numerical models involve mixed finite element and boundary element approaches [8,9]. Even though open infinite domains are quite natural for mixed models, an approach using finite element method is preferable since it involves sparse matrices (leading to reductions in terms of CPU time and memory requirements).

Most mathematical models use a harmonic approximation (limiting ourselves to principal harmonics of electric and magnetic field strength) to evaluate the electromagnetic

* Corresponding author.
E-mail address: dept13@iapmm.lviv.ua (B. Drobenko).

0017-9310/$ - see front matter © 2006 Elsevier Ltd. All rights reserved.
doi:10.1016/j.ijheatmasstransfer.2006.07.013

Nomenclature

$\mathbf{B}$	magnetic induction, $\mathbf{B} = (B_r(r,z,t), 0, B_z(r,z,t))$
$\mathbf{B}_*$	function relating induction and strength vectors for magnetic fields in a solid
$\mathbf{D}$	electric induction, $\mathbf{D} = (0, D_\varphi(r,z,t), 0)$
$\mathbf{D}_*$	function relating induction and strength vectors for electric fields in a solid
$\mathbf{D}$	strength of electric fields, $\mathbf{D} = (0, D_\varphi(r,z,t), 0)$
$\{E_h\}$	electric field strength in the nodes of the finite element mesh
$\mathbf{H}$	strength of magnetic fields, $\mathbf{H} = (H_r(r,z,t), 0, H_z(r,z,t))$
$H^1(\Omega)$	Sobolev's space, $H^1(\Omega) = \{w \in L^2(\Omega), \nabla w \in L^2(\Omega)\}$
c	heat capacity
$\mathbf{j}$	current density
J_0	maximum value of the current
$2L$	length of finite cylinder
$2L_i$	length of cylinder inductor
$\mathbf{n}$	unit vector normal to solid's surface Γ, $\mathbf{n} = (n_r, n_z)$
$[N]$	matrix of element's shape functions
Q_*	heat source averaged over period of electromagnetic field
R	radius of electric-conductive cylinder
R_i	radius of cylinder inductor
r, φ, z	cylindrical coordinates
T	temperature
$T_0(r,z)$	initial temperature in the solid
T_C	Curie point
$\{T_h\}$	temperature in the nodes of the finite element mesh
T_S	temperature of external medium
T_ω	period of electromagnetic field
V	finite volume substituting infinite space

Greek symbols

β	heat exchange coefficient
Δt_E	time step for electromagnetic calculations
Δt_T	time step for temperature calculations
ε	differential dielectric permeability of solid
ε_0	dielectric permeability of vacuum
γ	coefficient of electrical conductivity
Γ	surface of region occupying by solid
η	parameter characterizing time to reach steady regime
λ	coefficient of heat conduction
μ	differential magnetic permeability of solid
μ_0	magnetic permeability of vacuum
$\mu_{T_{20}}$	magnetic permeability averaged over the range of magnetic field strength at $T = 20\ ^\circ C$
ω	frequency
Ω	region occupying by solid
Ω^{el}	region occupying by finite element

field in the solid subjected to external harmonic electromagnetic field. This approximation is valid for linear magnetic materials but can become inaccurate when dealing with non-linear magnetic materials [3,6].

In this paper, the mathematical model and numerical investigation of non-stationary coupled electromagnetic and thermal processes in polarizable and magnetizable electro-conductive solids subjected to electromagnetic field generated by external currents are developed. Electromagnetic field in the solid and in the external medium is described by Maxwell's equations. Temperature evolution in the solid is governed by the classical heat transfer equation. The model takes into account the temperature dependence of all material coefficients and the non-linear dependence of induction on the strength of both electrical and magnetic fields. In a course of numerical investigation these dependencies are approximated by interpolation splines constructed by real curves describing temperature behavior of a solid during the entire heating–cooling range.

2. The mathematical problem

Consider axisymmetric electro-conductive solid occupying region Ω. The solid is subjected to electromagnetic field generated by coaxial with the solid currents of density $\mathbf{j}^{(0)} = (0, j_\varphi^{(0)}(r,z,t), 0)$ located in finite subdomain of external medium. Electromagnetic and temperature fields in the solid in the case of the following state equations:

$$\mathbf{B}^{(1)} = \mathbf{B}_*(\mathbf{H}^{(1)}, T), \quad \mathbf{D}^{(1)} = \mathbf{D}_*(\mathbf{E}^{(1)}, T),$$
$$\mathbf{j}^{(1)} = \gamma \mathbf{E}^{(1)}, \quad \mathbf{B}^{(0)} = \mu_0 \mathbf{H}^{(1)}, \quad \mathbf{D}^{(0)} = \varepsilon_0 \mathbf{E}^{(0)} \tag{1}$$

are described by coupled equations

$$\operatorname{curl} \mathbf{H}^{(m)} = \frac{\partial \mathbf{D}^{(m)}}{\partial t} + \mathbf{j}^{(m)}, \quad \operatorname{curl} \mathbf{E}^{(m)} = -\frac{\partial \mathbf{B}^{(m)}}{\partial t}, \tag{2}$$

$$c\frac{\partial T}{\partial t} = \frac{1}{r}\frac{\partial}{\partial r}\left(\lambda r \frac{\partial T}{\partial r}\right) + \frac{\partial}{\partial z}\left(\lambda \frac{\partial T}{\partial z}\right) + \mathbf{j}^{(1)}\mathbf{E}^{(1)}. \tag{3}$$

Here indexes $m = 0$ and $m = 1$ refer to external medium and the solid, respectively.

Let us reduce the basic correlations (2) for electro-conductive solid to a set of equations written with respect to electric field strength vector $\mathbf{E}$. Substitution of Eqs. (1) in (2) yields for the solid:

$$\operatorname{curl} \mathbf{H}^{(1)} = \varepsilon \frac{\partial \mathbf{E}^{(1)}}{\partial t} + \frac{\partial D_{*\varphi}^{(1)}}{\partial T}\frac{\partial T}{\partial t} + \gamma \mathbf{E}^{(1)}, \tag{4}$$

$$\operatorname{curl} \mathbf{E}^{(1)} = -[\mu_*]\frac{\partial \mathbf{H}^{(1)}}{\partial t} - \frac{\partial \mathbf{B}_*^{(1)}}{\partial T}\frac{\partial T}{\partial t}. \tag{5}$$

Here

$$[\mu_*] = \begin{bmatrix} \mu_r & \mu_{rz} \\ \mu_{zr} & \mu_z \end{bmatrix}; \quad \mu_r = \frac{\partial \mathbf{B}_{*r}^{(1)}}{\partial H_r^{(1)}}, \quad \mu_z = \frac{\partial \mathbf{B}_{*z}^{(1)}}{\partial H_z^{(1)}},$$
$$\mu_{rz} = \frac{\partial \mathbf{B}_{*r}^{(1)}}{\partial H_z^{(1)}}, \quad \mu_{zr} = \frac{\partial \mathbf{B}_{*z}^{(1)}}{\partial H_r^{(1)}}; \quad \varepsilon = \frac{\partial D_{*\varphi}^{(1)}}{\partial E_\varphi^{(1)}}.$$

Note that in the case of harmonic quasi-steady external electromagnetic field at condition $\gamma \gg \varepsilon\omega$, the displacement currents are negligible compared to conduction currents in a solid [10]. This is the case for the range of frequencies typically used in industrials set-up when we deal with highly conductive solids. Hence Eq. (4) becomes:

$$\operatorname{curl} \mathbf{H}^{(1)} = \gamma \mathbf{E}^{(1)}. \tag{6}$$

Let us restrict ourselves by the case of an isotropic solid ($\mu_r = \mu_z = \mu$, $\mu_{rz} = \mu_{zr} = 0$), whose differential magnetic permeability μ is directly derived – at a given temperature – from the magnetization curve, given by function $\mathbf{B}_*(\mathbf{H}, T)$ in (1).

Multiply Eq. (5) by μ^{-1}, take curl from both its side and account for Eq. (6). Then equation for the only non-zero component $E_\varphi^{(1)}$ of the electric field strength $\mathbf{E}^{(1)}$ in the solid takes a form:

$$-\frac{\partial}{\partial r}\left(\mu^{-1}\frac{1}{r}\frac{\partial}{\partial r}(rE_\varphi^{(1)})\right) - \frac{\partial}{\partial z}\left(\mu^{-1}\frac{\partial E_\varphi^{(1)}}{\partial z}\right) + \gamma\frac{\partial E_\varphi^{(1)}}{\partial t} = F_\mathrm{p}, \tag{7}$$

where

$$F_\mathrm{p} = \frac{\partial}{\partial r}\left(\frac{1}{\mu}\frac{\partial \mathbf{B}_{*z}}{\partial T}\frac{\partial T}{\partial t}\right) - \frac{\partial}{\partial z}\left(\frac{1}{\mu}\frac{\partial \mathbf{B}_{*r}}{\partial T}\frac{\partial T}{\partial t}\right).$$

Correspondent equation for a surrounding medium is as follows:

$$-\frac{1}{\mu_0}\left(\frac{\partial}{\partial r}\left(\frac{1}{r}\frac{\partial}{\partial r}(rE_\varphi^{(0)})\right) - \frac{\partial}{\partial z}\left(\frac{\partial E_\varphi^{(0)}}{\partial z}\right)\right) + \varepsilon_0\frac{\partial^2 E_\varphi^{(0)}}{\partial t^2} = -\frac{\partial j_\varphi^{(0)}}{\partial t}. \tag{8}$$

Electric filed strength in a system solid-surroundings being known, the magnetic field induction is found from the relations:

$$B_r^{(m)} = \int_0^t \frac{\partial E_\varphi^{(m)}}{\partial z}\,\mathrm{d}t', \quad B_z^{(m)} = -\int_0^t \frac{1}{r}\frac{\partial (rE_\varphi^{(m)})}{\partial r}\,\mathrm{d}t'. \tag{9}$$

The common practice is to start with integral form of Maxwell's equations in establishing the correlations for electromagnetic filed characteristics on solid-surroundings interface Γ. These correlations, provided surfacial currents are absent, yield two independent conditions expressing equality of tangential components of electric and magnetic field strength vectors on the interface [11]. In our case these conditions are

$$E_\varphi^{(1)} = E_\varphi^{(0)}, \tag{10}$$

$$\left(\mu^{-1}\frac{1}{r}\frac{\partial\left(rE_\varphi^{(1)}\right)}{\partial r} - \mu_0^{-1}\frac{1}{r}\frac{\partial\left(rE_\varphi^{(0)}\right)}{\partial r}\right)n_r + \left(\mu^{-1}\frac{\partial E_\varphi^{(1)}}{\partial z} - \mu_0^{-1}\frac{\partial E_\varphi^{(0)}}{\partial z}\right)n_z = 0. \tag{11}$$

Suppose the solid undergoes convective heat exchange with external medium through the interface Γ:

$$\lambda\left(\frac{\partial T}{\partial r}n_r + \frac{\partial T}{\partial z}n_z\right) + \beta(T - T_\mathrm{S}) = 0. \tag{12}$$

Put the following condition at the infinity and on the z-axis

$$E_\varphi = 0. \tag{13}$$

Suppose at initial moment of time there is no electromagnetic field in the system while the temperature in the solid is defined by known function $T_0(r, z)$. Then the problem of determination electromagnetic field in the system solid-surroundings reduces to solving set of Eqs. (3) and (7) for the solid and Eq. (8) for surroundings with zero initial value of electric field strength, given initial temperature distribution $T_0(r, z)$ in the solid, interface conditions (10)–(12), as well as conditions (13) at the infinity and the z-axis. In doing so, components of magnetic induction $\mathbf{B}$ are determined from (9), while magnetic field induction $\mathbf{H}$ as well as differential magnetic permeability μ in the solid in each moment of time are calculated using magnetization curve (1).

If we chose magnetic field strength $\mathbf{H}$ as a key function in determination electromagnetic field, we would get two equations (with $H_r(r, z, t)$, $H_z(r, z, t)$ unknown) to be solved together with Eq. (3), instead of single Eq. (6). However, if a long electro-conductive cylinder is subjected to quasi-steady external electromagnetic field independent of z-coordinate, the only component H_z is non-zero being determined from the following equation (neglecting displacement currents in the solid):

$$\frac{1}{r}\frac{\partial}{\partial r}\left(r\frac{1}{\gamma}\frac{\partial H_z^{(1)}}{\partial r}\right) - \mu\frac{\partial H_z^{(1)}}{\partial t} = \frac{\partial \mathbf{B}_{*z}}{\partial T}\frac{\partial T}{\partial t}. \tag{14}$$

If the interface value of $H_z^{(1)}$ is known the problem of determination electromagnetic field and the temperature in a cylinder reduces to solving Eq. (14) and

$$c\frac{\partial T}{\partial t} = \frac{1}{r}\frac{\partial}{\partial r}\left(\lambda r\frac{\partial T}{\partial r}\right) + j_\varphi^{(1)}E_\varphi^{(1)}, \tag{15}$$

$$E_\varphi^{(1)} = \frac{1}{\gamma}\frac{\partial H_z^{(1)}}{\partial r}. \tag{16}$$

Suppose in an initial moment of time the magnetic field is absent, function $T_0(r)$ defines initial temperature distribution while interface undergoes convective heat exchange:

$$-\lambda\frac{\partial T}{\partial r} = \beta(T - T_\mathrm{S}) \text{ at } r = R. \tag{17}$$

Also,

$$\frac{\partial T}{\partial r}=0,\quad \frac{\partial H_z^{(1)}}{\partial r}=0\quad \text{at } r=0. \tag{18}$$

The temperature T and the magnetic field strength $H_z^{(1)}$ being known, the differential magnetic permeability $\mu(H_z^{(1)},T)$ of a solid in each moment of time is found from magnetization curve.

3. The solution procedure

The solution of the posed problem is constructed using weighted residuals method [12]. With this purpose let us multiply heat transfer Eq. (3) by arbitrary weight function $w\in H^1(\Omega)$ and integrate obtained equation over domain Ω.

On using Green's formulae and accounting for heat exchange conditions (12), we get

$$\int_\Omega\left(c\frac{\partial T}{\partial t}w+\lambda\left(\frac{\partial T}{\partial r}\frac{\partial w}{\partial r}+\frac{\partial T}{\partial z}\frac{\partial w}{\partial z}\right)-j_\varphi^{(1)}E_\varphi^{(1)}w\right)r\,\mathrm{d}r\,\mathrm{d}z+\int_\Gamma\beta(T-T_\mathrm{S})wr\,\mathrm{d}\xi=0,\quad \forall w\in H^1(\Omega). \tag{19}$$

Let us apply the same approach to Eqs. (7) and (8), substituting the infinite space by a finite volume $V(\Omega\subset V)$ restricted by surface S located far enough from the solid and given currents. Having accounted for Green's formulae, we arrive at the equations:

$$\begin{aligned}&\int_\Omega\mu^{-1}\left(\frac{1}{r}\frac{\partial(rE_\varphi^{(1)})}{\partial r}\frac{1}{r}\frac{\partial(rw_1)}{\partial r}+\frac{\partial E_\varphi^{(1)}}{\partial z}\frac{\partial w_1}{\partial z}\right)r\,\mathrm{d}r\,\mathrm{d}z\\&+\int_\Gamma\mu^{-1}\left(\frac{1}{r}\frac{\partial(rE_\varphi^{(1)})}{\partial r}n_r+\frac{\partial E_\varphi^{(1)}}{\partial z}n_z\right)w_1r\,\mathrm{d}\xi\\&+\int_\Omega\left(\gamma\frac{\partial E_\varphi^{(1)}}{\partial t}-F_\mathrm{p}\right)w_1r\,\mathrm{d}r\,\mathrm{d}z=0\quad\forall w_1\in H^1(V);\end{aligned} \tag{20}$$

$$\begin{aligned}&\int_{V\setminus\Omega}\mu_0^{-1}\left(\frac{1}{r}\frac{\partial(rE_\varphi^{(0)})}{\partial r}\frac{1}{r}\frac{\partial(rw_1)}{\partial r}+\frac{\partial E_\varphi^{(0)}}{\partial z}\frac{\partial w_1}{\partial z}\right)r\,\mathrm{d}r\,\mathrm{d}z\\&+\int_{V\setminus\Omega}\varepsilon_0\frac{\partial^2E_\varphi^{(0)}}{\partial t^2}w_1r\,\mathrm{d}r\,\mathrm{d}z\\&-\int_\Gamma\mu_0^{-1}\left(\frac{1}{r}\frac{\partial(rE_\varphi^{(0)})}{\partial r}n_r+\frac{\partial E_\varphi^{(0)}}{\partial z}n_z\right)w_1r\,\mathrm{d}\xi\\&+\int_{V\setminus\Omega}\frac{\partial j_\varphi}{\partial t}w_1r\,\mathrm{d}r\,\mathrm{d}z=0\quad\forall w_1\in H^1(V).\end{aligned} \tag{21}$$

We get "−" sign in Eq. (21) since **n** is an internal normal to surface S relative to surrounding medium $V\setminus\Omega$.

Accounting for boundary conditions (11) and (12), we get the equation valid for the entire domain V:

$$\begin{aligned}&\int_V\mu_c^{-1}\left(\frac{1}{r}\frac{\partial(rE_\varphi)}{\partial r}\frac{1}{r}\frac{\partial(rw_1)}{\partial r}+\frac{\partial E_\varphi}{\partial z}\frac{\partial w_1}{\partial z}\right)r\,\mathrm{d}r\,\mathrm{d}z\\&+\int_V\left(F_\mathrm{c}\frac{\partial E_\varphi}{\partial t}+\varepsilon_\mathrm{c}\frac{\partial^2E_\varphi}{\partial t^2}+F_\mathrm{d}\right)w_1r\,\mathrm{d}r\,\mathrm{d}z=0\quad\forall w_1\in H^1(V),\end{aligned} \tag{22}$$

with the following notations:

$$\begin{cases}\mu_\mathrm{c}=\mu;\quad \varepsilon_\mathrm{c}=\varepsilon;\quad F_\mathrm{c}=\gamma;\quad F_\mathrm{d}=-F_\mathrm{p};\quad E_\varphi=E_\varphi^{(1)}\ \text{ for }\ (r,z)\in\Omega;\\ \mu_\mathrm{c}=\mu_0;\quad \varepsilon_\mathrm{c}=\varepsilon_0;\quad F_\mathrm{c}=0;\quad F_\mathrm{d}=\frac{\partial j_\varphi}{\partial t};\quad E_\varphi=E_\varphi^{(0)}\ \text{ for }\ (r,z)\in V/\Omega.\end{cases}$$

Apply typical finite element discretization of Eqs. (19) and (22) over spacial variables [12]. In doing so, discretization of the domain V is done in such a way that the solid-surrounding medium interface coincides with the boundaries of respective finite elements. As a result, a set of ordinary differential equations is obtained:

$$[L_1]\{\dot T_h(t)\}+[L_0]\{T_h(t)\}=\{f_T\},\quad \{T_h(0)\}=\{T_h^0\} \tag{23}$$

$$[M_2]\{\ddot E_h(t)\}+[M_1]\{\dot E_h(t)\}+[M_0]\{E_h(t)\}=\{f_E\},\quad \{E_h(0)\}=0,\quad \{\dot E_h(0)\}=0. \tag{24}$$

Matrix–vector characteristics of derived set of equations are calculated by summing up appropriate characteristics of finite elements:

$$\begin{aligned}[L_0]^\mathrm{el}&=\int_{\Omega^\mathrm{el}}\lambda\left(\left[\frac{\partial N}{\partial r}\right]'\left[\frac{\partial N}{\partial r}\right]+\left[\frac{\partial N}{\partial z}\right]'\left[\frac{\partial N}{\partial r}\right]\right)r\,\mathrm{d}r\,\mathrm{d}z+\int_{\Gamma^\mathrm{el}}\beta[N]'[N]r\,\mathrm{d}\xi,\\[L_1]^\mathrm{el}&=\int_{\Omega^\mathrm{el}}c[N]'[N]r\,\mathrm{d}r\,\mathrm{d}z,\\\{f_T\}^\mathrm{el}&=\int_{\Omega^\mathrm{el}}j_\varphi^{(1)}E_\varphi^{(1)}[N]'r\,\mathrm{d}r\,\mathrm{d}z+\int_{\Gamma^\mathrm{el}}\beta[N]'r\,\mathrm{d}\xi,\\[M_0]^\mathrm{el}&=\int_{V^\mathrm{el}}\frac{1}{\mu_\mathrm{c}}\left(\left[\frac{\partial N}{\partial r}\right]'\left[\frac{\partial N}{\partial r}\right]+\left[\frac{\partial N}{\partial z}\right]'\left[\frac{\partial N}{\partial z}\right]+\frac{1}{r}\left(\left[\frac{\partial N}{\partial r}\right]'[N]+[N]'\left[\frac{\partial N}{\partial r}\right]+\frac{1}{r}[N]'[N]\right)\right)r\,\mathrm{d}r\,\mathrm{d}z\\[M_1]^\mathrm{el}&=\int_{V^\mathrm{el}}F_\mathrm{c}[N]'[N]r\,\mathrm{d}r\,\mathrm{d}z,\\[M_2]^\mathrm{el}&=\int_{V^\mathrm{el}}\varepsilon_\mathrm{c}[N]'[N]r\,\mathrm{d}r\,\mathrm{d}z,\\\{f_E\}^\mathrm{el}&=\int_{V^\mathrm{el}}F_\mathrm{d}[N]'r\,\mathrm{d}r\,\mathrm{d}z.\end{aligned}$$

Here prime means transposing.

In the case of long cylindrical solid the problem (14)–(18) is reduced to a set of ordinary differential equations in a similar way.

Cauchy problem (23) and (24) is solved by use of a unified set of single step algorithms [13], what allows to carry out calculations for variable steps and orders of the method.

The solving of equations of electromagnetic and temperature fields with the same time step seems very ineffective in the case of harmonic electromagnetic loadings because temperature fields are much more inertial compared to electromagnetic ones. Therefore developed general algorithm allows to use different time steps for electromagnetic (Δt_E) and temperature (Δt_T) calculations (the method of ultra-weak coupling between both non-linear

time-dependent fields) [1,16]. Then averaged over the period of electromagnetic field heat source:

$$Q_* = \frac{1}{T_\omega}\int_0^{T_\omega} j_\varphi^{(1)} E_\varphi^{(1)}\,\mathrm{d}t,$$

is used in thermal conductivity equation.

4. Results and discussion

Consider high temperature induction heating of finite electric-conductive cylinder of radius R, and length $2L_i$. The cylinder is located in coaxial inductor of radius R_i and length $2L_i$ with current density given by expression:

$$\mathbf{j}^{(0)}(r,z,t) = (0, J_0(1-\mathrm{e}^{-\eta t})\cdot\sin(2\pi\omega t), 0);\quad r = R_i,\ |z| \leqslant L_i. \tag{25}$$

4.1. Non-poralizable and non-magnetizable material

We carried out computations for stainless steel with following characteristics taken from [11] ($\mu = \mu_0$; $\gamma = 1.35 \times 10^6$ S/m; $\lambda = 16.7$ W/(m K); $c = 3.957 \times 10^6$ J/(m^3 E); $\beta = 167$ W/(m^2 K); $J_0 = 6 \times 10^4$ A/m; $\omega = 3 \times 10^4$ Hz; $\eta = 10^7$ Hz; $T_0 = T_S = 0$) and compared our results with those of [11].

In Fig. 1 used typical finite element meshes are shown ($R = 0.01$ m; $L = 0.04$ m; $R_i = 0.012$ m; $L_i = 0.042$ m; $R_0 = 2.5R$; $L_0 = 2L$).

To examine convergence of numerical procedures the computations at various finite element meshes, time steps and sizes of domain V were carried out.

In Fig. 2(a) averaged heat sources Q_* along the radius of a long cylinder obtained in a closed form in [11] are shown by solid line. Here are also shown heat sources in cross section $z = 0$ of the cylinder, obtained on meshes 20×80, 10×40 (solid lines), 5×20 (∘) and 3×12 (×) of eight-node biquadratic isoparametric finite elements, at time step $\Delta t_E = T_\omega/32$ for electromagnetic calculations. Numerical results obtained on meshes 20×80 and 10×40 practically coincide with analytical solution. It could be seen that already five biquadratic elements along cylinder radius (Fig. 1(b)) give good agreement of the results.

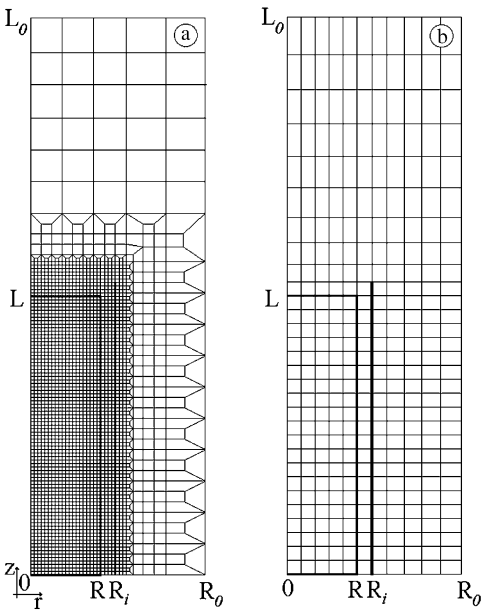

Fig. 1. Typical finite elements meshes.

In Fig. 2(b) curves 1–4 represent temperature distributions along cylinder radius in cross section $z = 0$ in moment of time $t = 7$ s. The results were obtained for thermal calculation with time steps $\Delta t_T = 0{,}209 \times 10^{-6}$ s ($T_\omega/16$); 1s ($\approx 10^5\ T_\omega$); 3,5 s ($\approx 10^6\ T_\omega$); 7s, respectively (curves 1–2 practically coincide). Note that temperature computation for this problem can be conducted with time step $\Delta t_T \geqslant 10^7 \Delta t_E$ without accuracy losses thus making it possible to find solutions of 2D problems for relatively short time. Specifically, solution of this transient 2D (in terms of spatial variables) problem at optimal finite element mesh (5×20) and time step $\Delta t_T = 1$s takes 4 s of ATHLON-2000 processor.

It should be pointed out that the substitution of surrounding medium by domain V with following parameters: $R_0 = 2.5R$, $L_0 = 2L$ (Fig. 1(b)) does not affect solution for the cylinder ($\forall R_0 > 2.5R$), $\forall L_0 > 2L$ solutions coincide; moreover in cross section $z = 0$ they practical coincide with analytical solution [11] and solution of 1D problem (14)–(18) for a long cylinder at boundary condition $H_z = 6 \times 10^4 \sin 2\pi\omega t$ A/m on a surface of the cylinder. These solutions tend to differ when $R_0 < 2.5R$, $L_0 < 2L$.

4.2. Ferromagnetic material

Consider induction heating of the cylinder made of low carbon (0.3%) steel. The cylinder ($R = 0.01$ m; $L = 0.1$ m) is heating by the current (25) ($R_i = 1.2R$; $L_i = 1.05L$; $J_0 = 10^6$ A/m^2; $\omega = 8 \times 10^3$ Hz; $\eta = 10^5$ Hz; $\beta = 13$ W/(m^2 K)). When external layer of thickness 1.5 mm in a cross section $z = 0$ of the cylinder is heated to the temperature $T \geqslant 970$ °C, the current is switched off and the cylinder is cooled down due to convective heat exchange ($\beta = 10^4$ W/(m^2 K)) with surrounding medium of the temperature $T_S = 20$ °C ($T_0 = T_S$).

Non-linear dependencies of magnetic induction on magnetic field strength are shown in Fig. 3(a) for the temperatures 20 (curve 1), 400 (2), 500 (3), 550 (4), 600 (5), 650 (6), 685 (7), 710 (8), 730 (9), 750 (10), 760 (11), 765 (12) °C. These dependencies, however, become linear with a coefficient μ_0 when the temperature is above Curie point T_C (770 °C) and steel loses ferromagnetic properties. Temperature dependencies of electrical conductivity, magnetic permeability, thermal conductivity as well as heat capacity are known [14,15].

Firstly let us determine transient temperatures in the cylinder within a model of a thermosensitive magnetic solid with the value of magnetic permeability [16]:

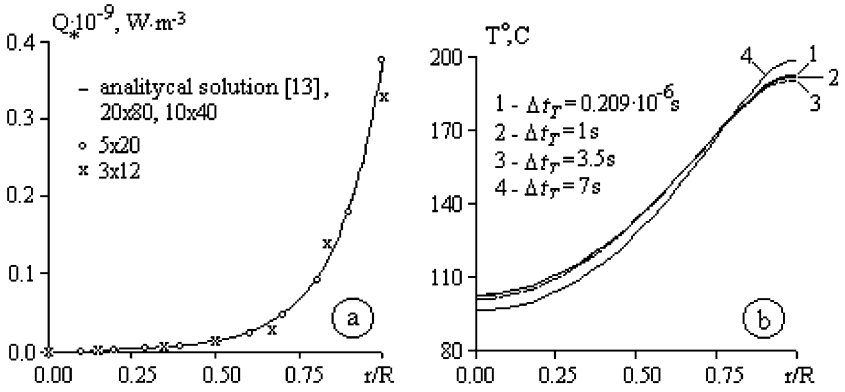

Fig. 2. Heat sources (a) and temperature (b) distributions in the cylinder ($t = 7$ s) for different number of elements and time steps.

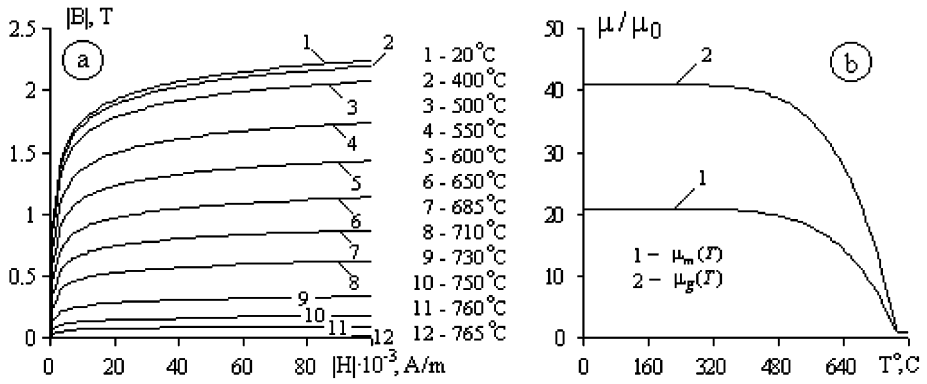

Fig. 3. Temperature dependencies of magnetic induction on magnetic field strength (a) and magnetic permeabilities averaged over the range of magnetic filed strength (b).

$$\mu_m(T) = \mu_0 + (\mu_{T_{20}} - \mu_0)\left(1 - \left(\frac{T}{T_C}\right)^6\right),$$

dependent on the temperature only (Fig. 3(b), curve 1). Here

$$\mu_{T_{20}} = \frac{1}{H_{\max}} \times \int_0^{H_{\max}} \mu(H, T|_{20\,^\circ C})\mathrm{d}H \quad \left(\mu(H,T) = \frac{\partial|B(H,T)|}{\partial|H|}\right),$$

is the magnetic permeability averaged over the range of magnetic field strength at $T = 20$ °C calculated from magnetization curve in Fig. 3(a) (curve 1).

4.2.1. Model of magnetic thermo-sensitive solid

In Fig. 4 isotherms T in the solid are shown in the moments of time when surface in cross section $z = 0$ is heated to T_C (to the left in Fig. 4) and the current is switched off (to the right in Fig. 4), respectively. Boundary effect in this case is spread over domain equal about six radii of the cylinder the same estimation of the boundary effect is got for $L = 0.2$ m; $L_i = 1.05L$. Solutions in the central section of the cylinder (in the vicinity of cross section $z = 0$) are, in fact, independent of z and coincide (within 1% accuracy) with correspondent solutions of 1D boundary-value problem (14)–(18), written in terms of magnetic field strength H_z.

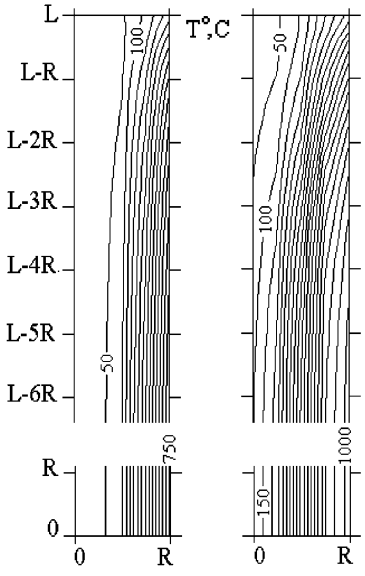

Fig. 4. Temperature distributions in the cylinder.

Effect of the temperature dependence of the steel electrical conductivity coefficient γ and magnetic permeability μ on temperature distributions in the cylinder was also

investigated. Temperature rise in time on cylinder surface for four characteristic cases are shown in Fig. 5: 1 – both coefficients are temperature dependent; 2 – electric conductivity coefficient is constant ($\gamma_m = 2.08 \times 10^6$ S/m), averaged over heating range, while magnetic permeability is temperature dependent; 3 – magnetic permeability μ is temperature independent and equal μ_{20} (at $T = 20$ °C), while electrical conductivity coefficient is temperature dependent; 4 – both coefficients are temperature independent. Already at the temperature around 300 °C consideration of temperature dependencies of electrical and physical characteristics is crucial. It becomes even more important with further heating of the cylinder. As the temperature approaches Curie point T_C (above 600 °C), heating of the surface slows down significantly what can be associated with sudden drop of steel magnetic permeability near Curie point.

Already twenty elements along cylinder radius with time step $\Delta t_E = T_\omega/16$ assure convergence of the solutions. However, obtained approximate values of magnetic field strength near Curie point differ considerably from exact solutions at such spatial approximation. In particular, the difference reaches 20% at forty elements over cylinder thickness while even more than 200% if number of elements is twenty. In Fig. 6 changes in time of maximum value of magnetic field strength on cylinder surface are shown when number of biquadratic elements at time step $\Delta t_E = \Delta t_T = T_\omega/32$ is twenty (curve 1), forty (curve 2), eighty (curve 3) and two hundreds (curve 4).

Twenty biquadratic elements over cylinder thickness are enough for computation temperature field – eighty elements give practically the same accuracy, in fact.

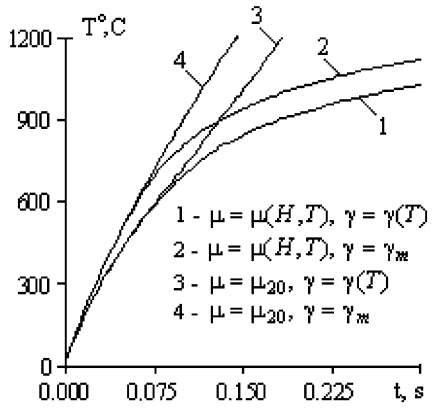

Fig. 5. Temperature rise in time on cylinder surface for different ways of simulation.

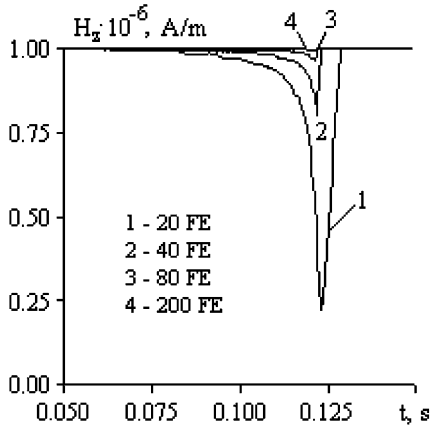

Fig. 6. Changes in time of maximum value of magnetic field strength on cylinder surface for different finite element meshes.

4.2.2. Model of ferromagnetic thermo-sensitive solid

In Figs. 7 and 8 curves 1–9 show profiles of maximum values of electric E_φ and magnetic H_z field strength and temperature along cylinder radius in a cross section $z = 0$ of a ferromagnetic cylinder during heating for moments of time $t = 0.007$; 0.02; 0.04; 0.06; 0.08; 0.1; 0.12; 0.14; 0.159 s. Because of temperature dependencies of electric and physical coefficients of steel the maximum values of electric and magnetic field strength change slowly period by period. At the initial phase of the heating the skin effect is clearly observed. However, magnetic field penetrates deeper as heating of external layers of the cylinder progresses. When they are heated to Curie point or above the loss of ferromagnetic properties causes considerable changes in parameters of processes in the cylinder. Maximum values of electric field strength (and heat sources power, respectively) move in the bulk of the cylinder so that maximum heat is released in the domains where ferromagnetic properties are not lost. In doing so, heating of surfacial layers slows down.

The current is switched off when cylinder is heated to 970 °C or above at needed depth in moment of time $t = 0.159$ s. Cylinder begins to cool down due to convective heat exchange with surrounding medium. Temperature change during cooling in cross section $z = 0$ with coordinated $r = 10$ (curve 1), 8 (2), 6 (3), 5 (4), 4 (5), 0 (6) mm are shown in Fig. 9. It is seen that core of the cylinder is still heated during $t = 2$ s after current being switched off due to thermal conductivity mechanism.

Numerical analysis indicates that a time step $\Delta t_E \geqslant \omega^{-1}/250$ assure the convergence of coupled electrodynamics and thermal conductivity problem solutions. In Fig. 10 distributions of the temperature in the cylinder in the moment of inductor switching off are shown for the following values of time discretization step Δt_E of electrodynamics equations: 0.5 μs (curve 1, corresponding to lowest temperatures in the bulk of the cylinder and highest ones on its surface); 0.25 μs (2); 0.05 μs (3); 0.01 μs (4). 400 bilinear elements used along cylinder radius.

Results for the duration of a heating of cylinder to needed temperature predicted by two considered models differ nearly by two times – 0.289 s is the prediction of the model of magnetic solid while ferromagnetic model gives 0.159 s. Because of that, a set of computations was carried out to find out such magnetic permeability independent of magnetic field strength:

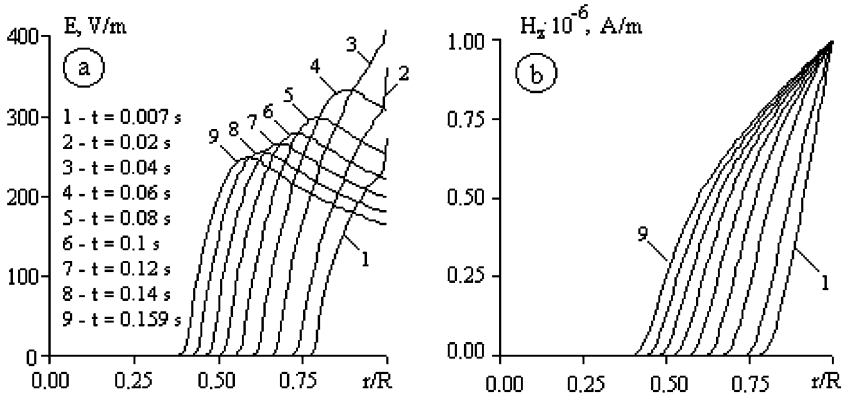

Fig. 7. Profiles of maximum values of electric (a) and magnetic (b) field strengths in the cylinder during heating.

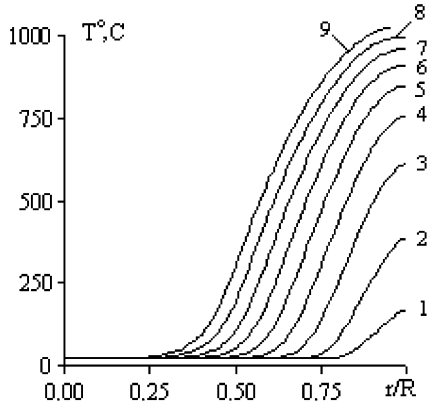

Fig. 8. Profiles of temperature in the cylinder during heating.

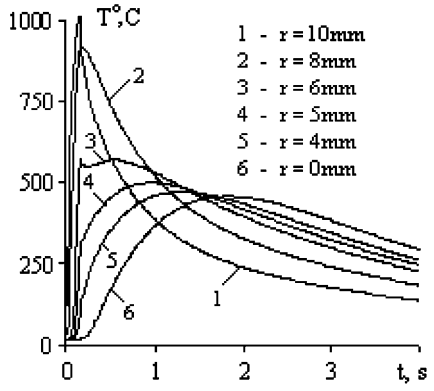

Fig. 9. Temperature changes during the process in different points of cylinder.

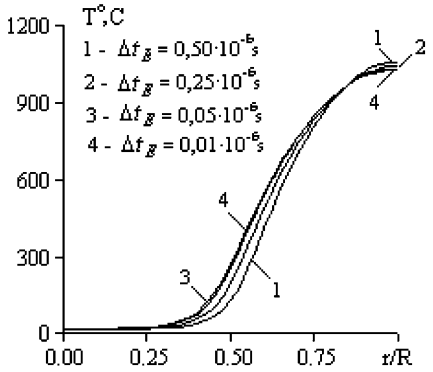

Fig. 10. Temperature distributions in the cylinder in the moment of inductor switching off for different time steps of electrodynamics calculations.

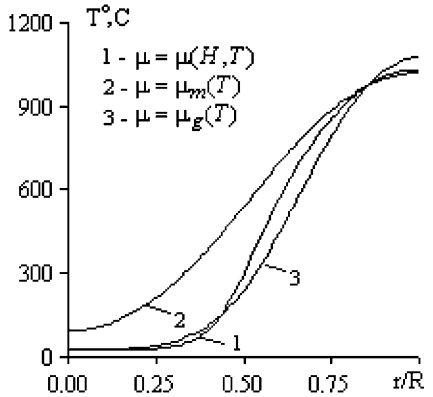

Fig. 11. Distributions of temperature in the cylinder in the moment of inductor switching off for different ways of simulation.

$$\mu_g(T) = \mu_0 + (\mu_{T_g} - \mu_0)\left(1 - \left(\frac{T}{T_C}\right)^6\right),$$

which would predict the same heating duration to a given temperatures by both models (temperature dependence of magnetic permeability μ_g is shown in Fig. 5, curve 2).

Figs. 11 and 12 illustrate distributions of maximum values of temperature, as well as electric and magnetic strengths in the moment of inductor switching off. Curve 1 was obtained within the model of ferromagnetic material while curves 2 and 3 were predicted by magnetic material model with respective magnetic permeabilities μ_m and μ_g dependent on the temperature only. It could be seen that it is possible to find out such magnetic permeability that would assure accurate enough electromagnetic field characteristics and correspondent temperatures in ferromagnetic cylinder.

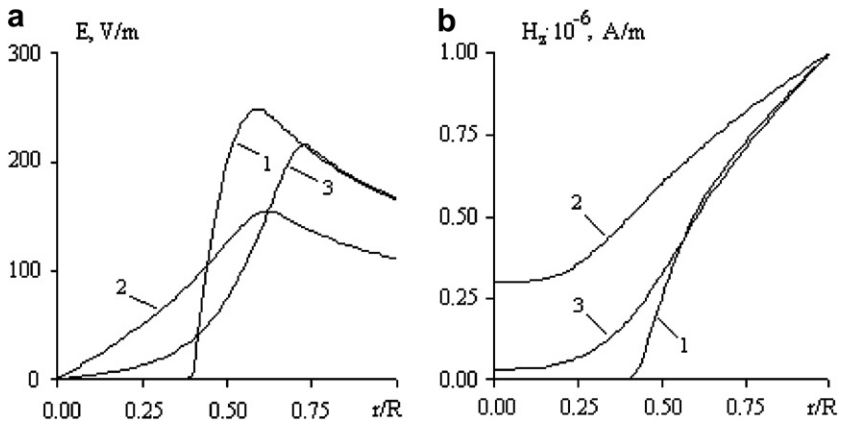

Fig. 12. Distributions of maximum values of electric (a) and magnetic (b) strengths in the cylinder in the moment of inductor switching off for different ways of simulation.

5. Conclusions

Numerical results obtained clearly indicate on the necessity to account for temperature dependencies of electric and magnetic characteristics in considered problems. In particular, neglecting of a temperature dependence of electric conductivity coefficient of low carbon steel considerably effects on a correctness of the solutions even at temperatures around 300 °C. Temperature dependence of magnetic permeability in the temperature range below 600 °C can be neglected.

Simulations for induction heating of other materials can also be done using developed approach as long as the relevant material properties are known.

Proposed approach to determination electromagnetic parameters and temperature in electro-conductive solid located in external electromagnetic field could be applied to analysis of stress–strain state of the solid, namely, to determination residual stresses due to induction heating. It can also be of use when optimum, by certain criteria, induction heating regimes are to be developed for electrically conductive materials, these criteria being particularly homogeneity of a heating, minimization of power expenses, residual stresses reduction, etc.

References

[1] F. Bay, V. Labbe, Y. Favennec, J.L. Chenot, A numerical model for Induction heating processes coupling electromagnetism and thermomechanics, International Journal for Numerical Methods in Engineering 58 (6) (2003) 839–867.

[2] O. Bodart, A.-V. Boureau, R. Touzani, Numerical investigation of optimal control of induction heating processes, Applied Mathematical Modelling 25 (2001) 697–712.

[3] C. Chaboudez, S. Clain, R. Glardon, D. Mari, J. Rappaz, M. Swierkosz, Numerical modelling in induction heating for axisymmetric geometries, IEEE Transactions on Magnetics 33 (1) (1997) 739–745.

[4] Y. Favennec, V. Labbe, F. Bay, A numerical modeling example in multiphysics coupling: Analysis and optimization of induction heating processes, Mecanique and Industries 4 (2003) 347–355.

[5] C. Marchand, A. Foggia, A 2-D finite element program for magnetic induction heating, IEEE Transactions on Magnetics 19 (6) (1983) 2647–2649.

[6] J. Rappaz, M. Swierkosz, Mathematical modelling and simulation of induction heating processes, Applied Mathematics and Computer Science 6 (2) (1996) 207–221.

[7] K. Sadeghipour, J.A. Dopkin, K. Li, A computer aided finite element/experimental analysis of induction heating process of steel, Computers in Industry 28 (1996) 195–205.

[8] T. Myoshi, M. Sumiya, H. Omori, Analysis of an induction heating system by the finite element method combined with the boundary integral equation, IEEE Transactions on Magnetics 23 (2) (1987) 1827–1832.

[9] S.J. Salon, J.M. Schneider, A hybrid finite element–boundary integral formulation of eddy current problem, IEEE Transactions on Magnetics MAG-18 (1982) 461–466.

[10] I.E. Tamm, The Basis of the electricity theory, Moscow, 1976, pp. 397–403 (in Russian).

[11] Ya.S. Podstryhach, Ya.Yo. Burak, A.R. Gachkevich, L.V. Cherniavskaya, Thermoelasticity of Electrically Conductive Solids, Kiev, Naukova Dumka, 1977, pp. 11–12, 126–132 (in Russian).

[12] O. Zenkievicz, K. Morgan, Finite Elements and Approximation [Russian translation], Mir, Moscow, 1986, pp. 40–92 (in Russian).

[13] O.C. Zienkiewicz, W.L. Wood, N.W. Nine, A unified set of single step algorithm. Part 1: General formulation and applications, International Journal for Numerical Methods in Engineering 20 (1984) 1529–1552.

[14] I.K. Kikoin (Ed.), Tables of Physical Values, Reference Book, Atomizdat, Moscow, 1976, p. 162, 264 pp. (in Russian).

[15] J. Turowski, Technical Electrodynamics, WNT, Warsaw, 1993, 30 pp. (in Polish).

[16] T. Skoczkowski, M. Kalus, The mathematical model of induction heating of ferromagnetic pipes, IEEE Transactions on Magnetics 25 (3) (1989) 2745–2750.